PERGAMON

International Journal of Multiphase Flow 26 (2000) 147–167

International Journal of Multiphase Flow

www.elsevier.com/locate/ijmulflow

Thermal patterns on a heated wall in vertical air–water flow

G. Hetsroni*, R. Rozenblit

Department of Mechanical Engineering, Technion, Israel Institute of Technology, Haifa, Israel

Received 1 February 1998; received in revised form 25 February 1999

Abstract

The thermal patterns on a heated wall, as related to the flow regime, were studied by using the heated foil infrared technique. The thermal pattern on the heated wall for the single-phase water flow has a streaky structure. For the bubble flow, the streaky structure is destroyed. This phenomenon is accompanied by a significant increase in the heat transfer coefficient. For the slug flow regime, the thermal pattern on the wall depends on whether water containing small gas bubbles (slug) or water surrounding a Taylor bubble passes the heated wall. Simultaneously, the temperature and pressure fluctuations at the wall were measured. The level of these fluctuations was discussed together with the data about the average heat transfer. The excess form of heat transfer coefficient was introduced. A correlation for the dimensionless heat transfer coefficient at slug flow was suggested.

Keywords: Two-phase flow; Thermal pattern; Heat transfer; Flow regime

1. Introduction

The heat transfer mechanism in two-phase flows attracts the attention of researchers and designers. The parameters of engineering interest, e.g. local and average heat transfer coefficients and wall temperature fluctuations, depend strongly on the flow regime and pressure fluctuations.

The investigations which have been done were usually focused on relations between flow

* Corresponding author. Tel.: +972-48-292-058; fax: +972-48-343-362.
E-mail address: hetsroni@tx.techion.ac.il (G. Hetsroni).

0301-9322/00/$ - see front matter
PII: S0301-9322(99)00015-4

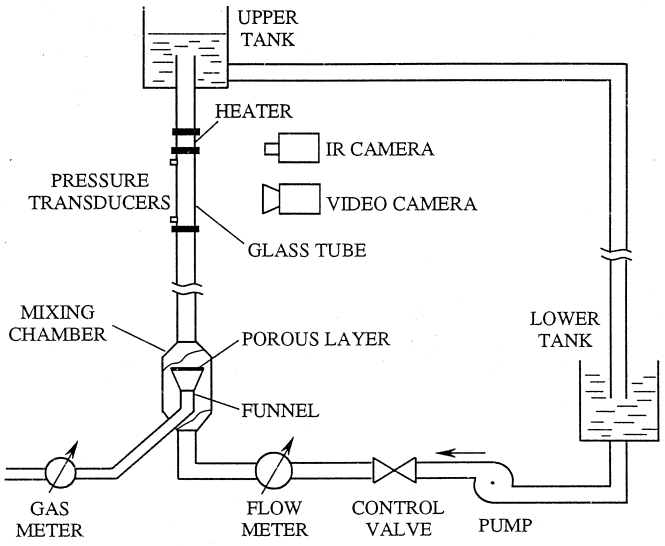

(a)

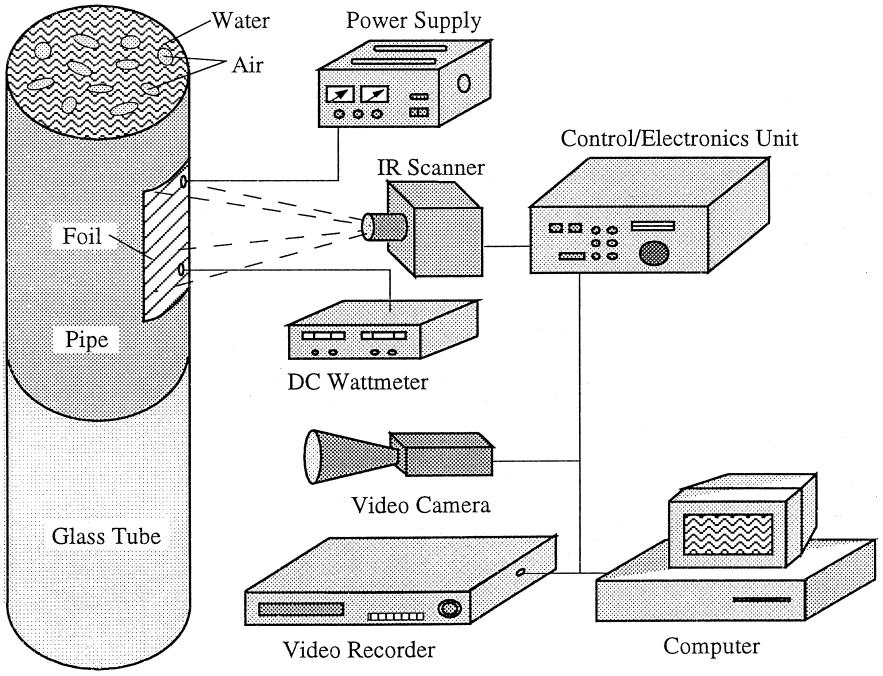

(b)

Fig. 1. Experimental set-up. (a) A schematic diagram of the loop; (b) test section and measurement scheme.

structure (flow patterns, phase and velocity distributions, etc.) and an average heat transfer coefficient. However, the experimental evidence for connecting the flow parameters to the thermal pattern on the wall does not exist.

This work is aimed at revealing the relations between fluctuating values of the pressure and temperature, the thermal structure on a heated wall and the heat transfer coefficient in the bubble and slug air–water flow.

2. Experimental

2.1. Experimental set-up

Experiments were carried out for a vertical upward air–water flow in a circular pipe of inner diameter 74 mm. The reasons for choosing this diameter were:

1. The large diameter provided the possibility to obtain more information about the behavior of thermal patterns on a heated wall of a test section.
2. Very stable bubble flow regime was reached.

A schematic diagram of the loop is shown in Fig. 1. The overall height of the set-up is 12 m. It includes a 8 m long entrance section (about 110 tube diameters), which makes it possible to obtain a fully developed turbulent flow in the test section. The water is provided by a pump (Fig. 1(a)), regulated by a bypass line and valves, and measured by an orifice. After leaving the flow meter, water flows into the pipe at the bottom end, then reaches a two-phase mixer. The mixing chamber is 900 mm long and 150 mm in inner diameter. Air is introduced continuously through a funnel with a porous layer in its end. The mean pore diameter is 120 μm. A two-phase bubbly mixture flows upward into the test section after passing through a transparent glass section serving for recognition of flow patterns. There are two high-accuracy pressure transducers at the ends of this glass tube at a distance 1.06 m apart.

After passing through the observation and pressure measurement section, the air–water mixture flows into the heated section. This part of the test section (Fig. 1(b)) is designed for visualization of thermal patterns on the heated wall and for temperature measurements. A constantan foil, 50 μm thick, is installed inside the polyethylene tube, which has windows cut in its wall, to make the foil visible to the IR radiometer. The window for IR observation is 90 mm long and 60 mm wide. The foil is coated, on the air side, by black mat paint of about 20 μm thickness. Constancy of heat flux is achieved by supplying DC power at up to 400 A.

Then, the mixture flows upward to the upper tank. The air is released into the atmosphere, while the water returns to the entrance tank, on the lowest level. The main purpose of this configuration is to provide better separation of the air from the water, in order to obtain well-controlled flow rates of both phases.

2.2. Measurement techniques

The IR measurement technique. A thermal imaging radiometer "Inframetrics model 760" is used for the investigation of the temperature distribution and thermal pattern on the heated

foil of the test section. It consists of a scanner and a control/electronics unit. The scanner incorporates electromechanical servos to perform horizontal and vertical scanning. Horizontal scanning is performed at a 4 kHz rate in a resonant (sinusoidal) mode. Vertical scanning is performed using a sawtooth pattern commensurate with standard television formats. A mercury/cadmium/telluride detector is cooled by an integrated cooler to 77 K for maximum thermal sensitivity and high spatial resolution. The control/electronics unit contains circuits to process, digitize and reformat the IR signal to display it in color or black and white on the built-in or external video monitor.

The temperature range of the radiometer is from -20 to 1500°C, with a minimum detectable temperature difference of 0.1°C at 30°C. Through calibration, the thermal imaging radiometer is very accurate in a narrow temperature range, giving the typical noise equivalent temperature difference (NETD) only, which is less than 0.2°C (with the image average less than 0.05°C). A typical horizontal resolution is 1.8 mrad or 256 pixels/line.

For all the performance characteristics mentioned above, it is assumed that the surface of the heater behaves as a black body, because the heater was coated with paint which is "black" in the IR range. The calibration of the radiometer was checked with a precision mercury thermometer placed in the water.

The radiometer facilitates obtaining a quantitative thermal profile in the "line mode", the average temperature in the "area mode", and the temperature of a given point in the "point mode".

Since the experiments were performed in two-phase flow, the heat transfer coefficient fluctuated in time. However, as was shown by Hetsroni and Rozenblit (1994), the temperature distortions and phase shift in temperature fluctuations on the heated foil begin at $f = 15$ Hz. In the present study the highest frequency of fluctuations did not exceed 6 Hz.

A special computer program made it possible to store the information on the temperature fluctuations. Simultaneously, the thermal pattern was recorded on a video tape. The video was then used in a playback mode to analyse the data.

The flow parameters measurement. The flow regime was defined by a video record analysis. The camera provided the video signal which consisted of two fields, represented by the odd and even rows of the image, respectively. For a PAL video system, the time interval between the two fields is 0.02 s.

The water flow was controlled by a valve and measured by a standard orifice plate with an accuracy of $\pm 1\%$. The air flow was measured by means of a mass flowmeter "Hastings model HFM" with an accuracy of $\pm 1\%$. The pressure was measured by the pressure transducers (series 692) with an accuracy of $\pm 1\%$ and response time of less than 5 ms. Electrical power was determined by means of a digital wattmeter with an accuracy of $\pm 0.5\%$. All data from sensors were transmitted to a PC, to be stored and analysed.

2.3. Experimental procedure

An experimental run consisted of establishing the flow rate with and without air at different values of heat flux. The values of flow parameters and heat flux used in this study are listed in the table.

Two-phase tests were conducted at constant liquid flowrates, with various air flowrates. The

experiments were repeated to confirm their reproducibility. The heat transfer and flow parameters for each run were measured under steady-state conditions.

The video image was used for identifying the air–water flow regime. The transparent tube was illuminated by a 500 W halogen lamp. Pictures were taken against a black background.

For each run the pressure measurement was carried out for both the upper and lower pressure transducers. The pressure fluctuations were measured by sensors with response time less than 5 ms at sampling frequency of 500 Hz.

The study of thermal pattern on a heated wall and local heat transfer coefficient was carried out in the following way. We placed the scanner of IR radiometer at the distance of about 0.7 m from the side of the test section and measured the average temperature of the heater, and the temperature fluctuations at the center of the heater. These measurements were carried out both with air flow and without it. During each run, a sequence lasting at least 200 s was stored. Simultaneously, the thermal pattern was recorded on a video cassette. The video was then used to determine the effect of pressure fluctuations and flow regime on the thermal pattern.

Preliminary calculations (Hetsroni and Rozenblit, 1994) have shown that the difference between the temperatures of the two sides of the thin constantan foil was less than 0.1°C. The estimated total heat losses were in the range of 1–2%, depending on the values of the heat flux.

The time-averaged heat transfer coefficient is defined as

$$\alpha = q\left(\bar{T}_w - T_f\right) \tag{1}$$

where q is the heat flux, $\bar{T}_w$ is the time-averaged wall temperature, T_f is the temperature of the water or air–water mixture, measured at $q = 0$.

Great care was taken to obtain a hydrodynamically developed bubble or slug flow. Naturally, a relatively short heater does not make it possible to fully develop the thermal boundary layer. However, in air–water flow the thermal conditions at the wall follow the intermittently changing two-phase flow. Hence, the question whether the thermal boundary layer is developed or not becomes less important.

3. Results

3.1. Pressure fluctuations

Two-phase flow regimes have been studied by a number of authors to obtain objective criteria for identification of various flow patterns. The applied methods include analysis of power spectral densities (psd), probability density function (pdf), fractal characteristics of detector signals, and various pattern recognition techniques (Vince and Lahey, 1982; Dukler and Taitel, 1986; Baba et al., 1991; Kozma et al., 1996, etc.).

The attempts to use the spectra of wall pressure fluctuations to describe various flow regimes in the case of horizontal flow were done by Hubbard and Dukler (1966). The wall pressure

fluctuations for vertical flow have been studied by Tutu (1984) to distinguish the boundaries of this transition.

It was shown (Jones and Zuber, 1975; Tutu, 1984; Costigan and Whalley, 1997) that only analysis of the pressure drop fluctuations or void fraction leads to clear quantitative criteria for bubble–slug transition. The careful definition of boundaries is an independent and difficult problem. Meanwhile, the study of pressure wall fluctuations together with temperature fluctuations can yield better knowledge of local heat transfer and related to it thermal structure at the heated wall.

The typical signals of two pressure transducers in bubble flow are shown in Fig. 2. Almost periodic oscillations can be seen for the upper transducer (Fig. 2(b)), while the oscillations measured by the lower transducer (Fig. 2(a)) appear to be similar, but with additional higher frequency variations. Fig. 3(a)–(b) shows pressure signals of transducers in slug flow.

Changes in the character of these signals were described by using power spectral densities (psd). In Fig. 4, the psd functions for bubble, bubble–slug and slug regime are shown.

There is a clear peak in the spectra measured at bubble flow, indicative of the presence of almost periodic oscillations. The frequency of these oscillations is about 5.7 Hz. The second peak appears at bubble–slug and slug flows. It has a very low frequency of about 0.7 Hz. Thus, a bimodal form of the flow pattern takes place. The bimodal form of signal related to pressure was described by Kozma et al. (1996), Costigan and Whalley (1997), and in a number of other works.

These measured signals were analysed also by using the probability density function (pdf).

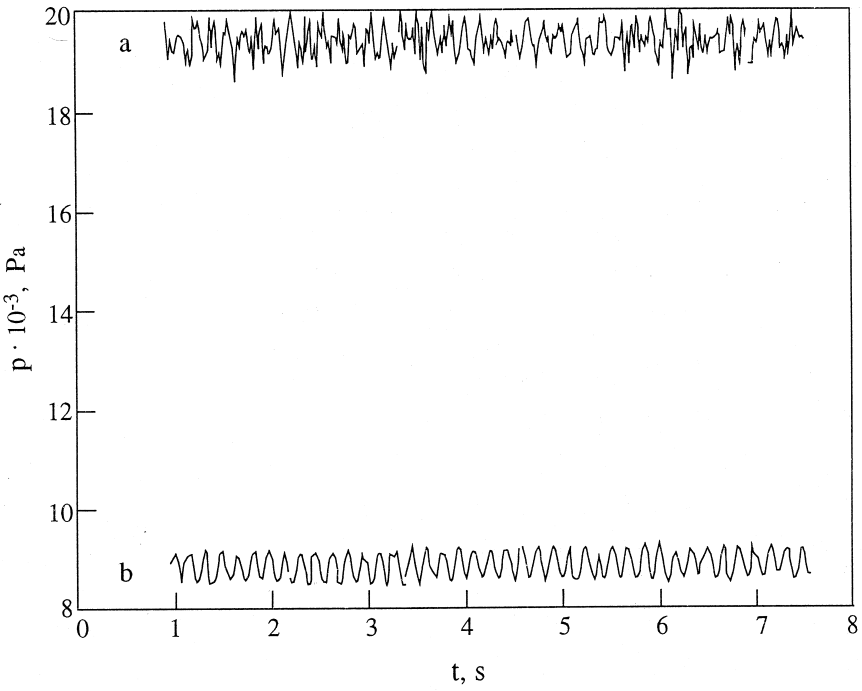

Fig. 2. The pressure transducer signals at bubble flow: (a) lower; (b) upper ($Re_L = 16{,}000$; $V_{GS}/V_{LS} = 0.08$).

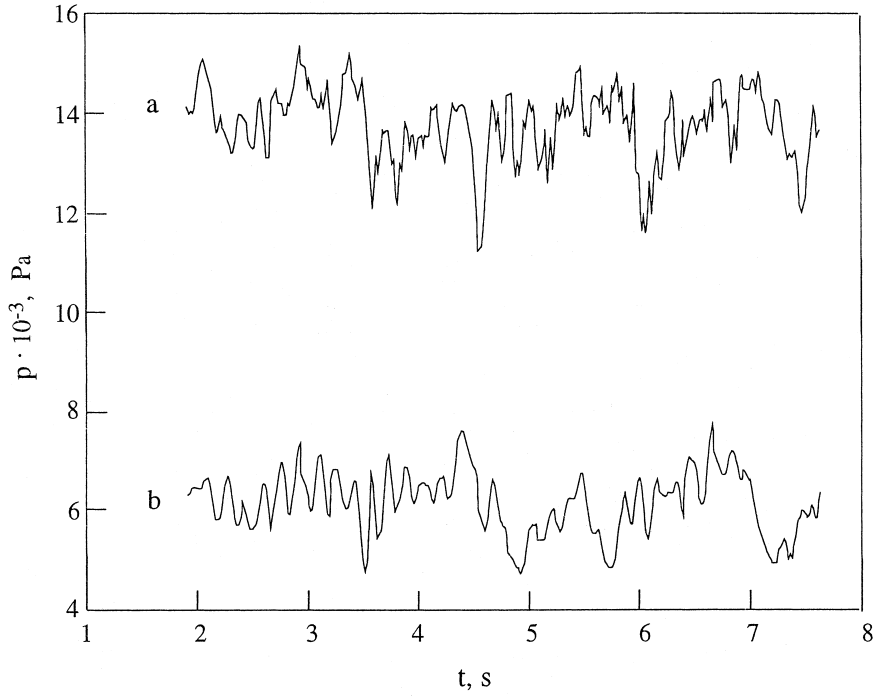

Fig. 3. The pressure transducer signals at slug flow: (a) lower; (b) upper ($\mathrm{Re}_L = 16{,}000$; $V_{GS}/V_{LS} = 1.15$).

Fig. 5(a) shows the pdf for the signal in bubble flow. The level ε of pressure fluctuations for the abscissa was normalized by their standard deviation (std). The std is the positive square root of the variance (the second moment about the mean). We see that the shape of the pdf does not fit the Gaussian distribution, which characterizes the random deviations about the mean. It becomes closer to the pdf of the sinusoidal fluctuations (dashed line), in accordance to the psd data of bubble flow discussed above. On the other hand, the data for slug flow agree (Fig. 5(b)) with the normal distribution fairly well, in spite of the existence of two maxima in the psd data.

The tendency to the existence of definite frequencies in air–water is related to the propagation velocity (Kosaly et al., 1982). Concerning the axial propagation of the pressure fluctuation δ_p, we consider a time delay behavior associated with a constant velocity V:

$$\delta p(t, z) = \delta p\left(t - \frac{z}{V}, 0\right). \tag{2}$$

In the frequency domain, (2) becomes

$$\delta p(\omega, z) = \mathrm{e}^{\mathrm{i}\omega z/V}\delta p(\omega, 0). \tag{3}$$

Eqs. (2) and (3) are valid only in adiabatic incompressible flow (Zuber and Staub, 1967; Wallis, 1969). However, this point can be accepted as a starting one.

It follows from (2) and (3) that

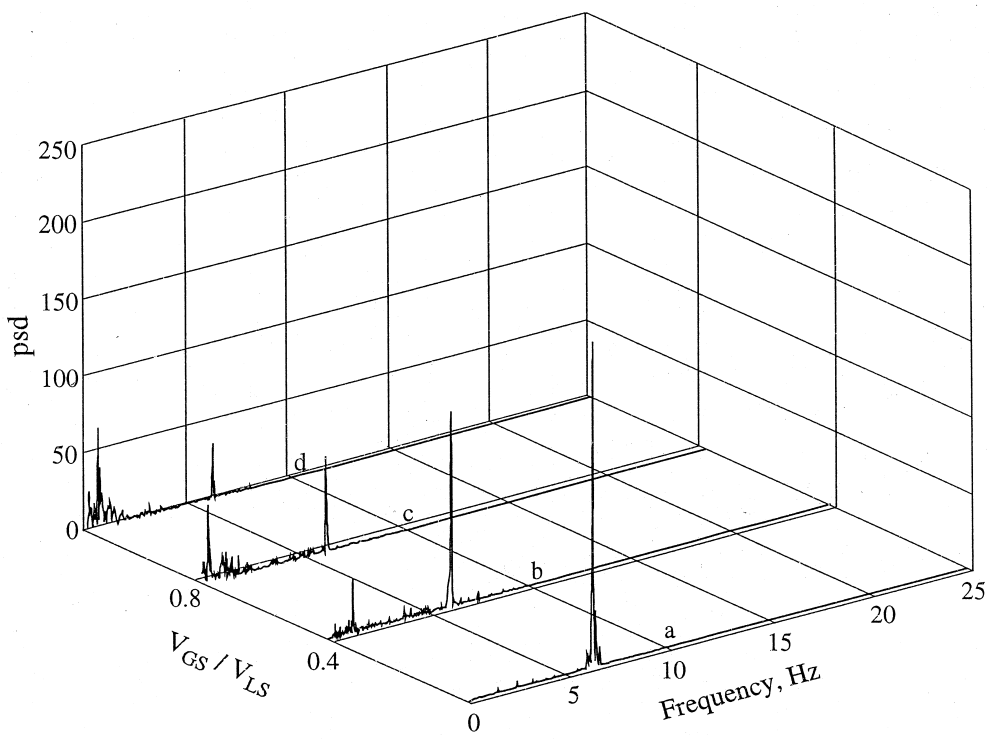

Fig. 4. Psd of the upper pressure transducer signal at various flow regimes ($Re_L = 16{,}000$): (a) bubble flow; (b) bubble + slug flow; (c), (d) slug flow.

$$\mathrm{CPSD}^{p}_{z_1,\,z_2}(\omega) = \mathrm{e}^{-\mathrm{i}\omega/V(z_2-z_1)} \cdot \mathrm{APSD}^{(p)}_{z_1}(\omega); \quad z_1 \leqslant z_2 \tag{4}$$

and

$$\mathrm{APSD}^{p}_{z}(\omega) = \mathrm{APSD}^{p}(\omega) \tag{5}$$

where CPSD and APSD are cross- and autospectrum of pressure signals, respectively. This means that (1) the phase of the cross-spectrum is linear with frequency; and (2) the autospectrum is independent of the position. Following Kosaly et al. (1982), we get the characteristic frequency as

$$f_s = 2V/H \tag{6}$$

where $H = 10$ m is the height of the tube, excluding the mixing section.

The large diameter and height of the pipe, as well as small friction, allow us to check this relation by using our experimental data. In Figs. 6(a)–(b), the cross-correlation coefficient R of pressure signals for bubble and slug flow are shown. There are two ways to define the characteristic frequency. We can find the time delay $\Delta\tau$ as a time where the first maximum of the cross-correlation coefficient R is reached, and after that the propagation velocity $V = l_0/\Delta\tau$, where $l_0 = 1.06$ m is the distance between the upper and lower transducers, and use (6).

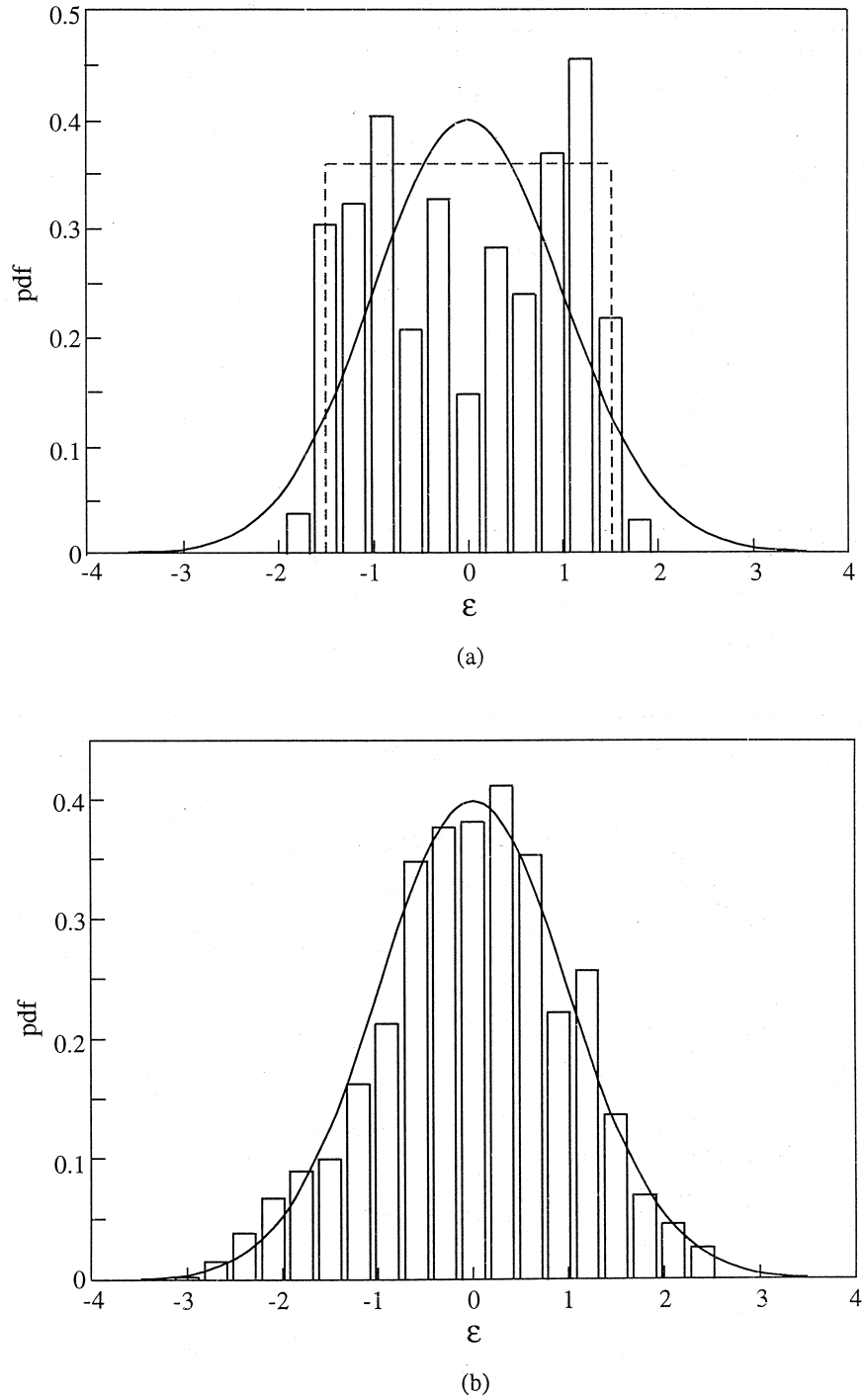

Fig. 5. Probability density function for the upper pressure transducer signal: (a) Bubble flow; (b) slug flow.

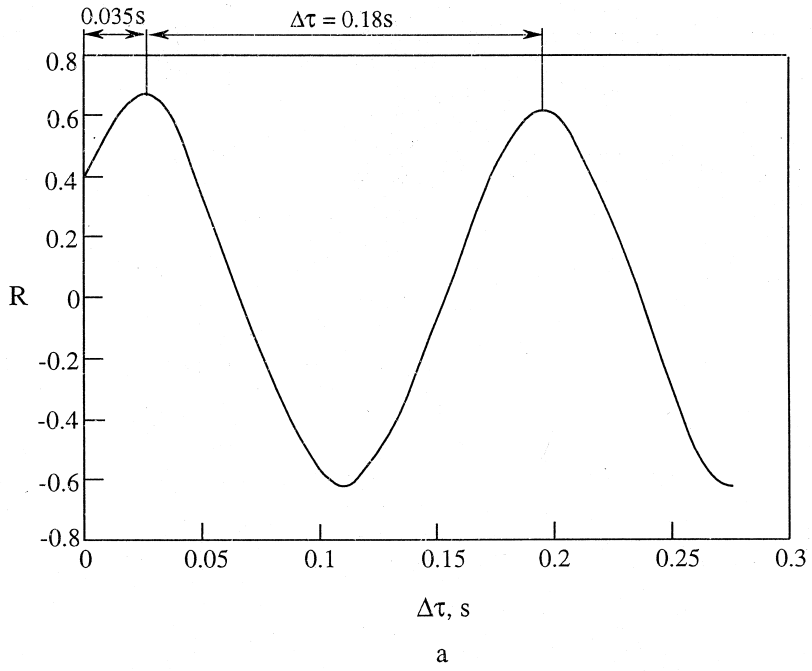

a

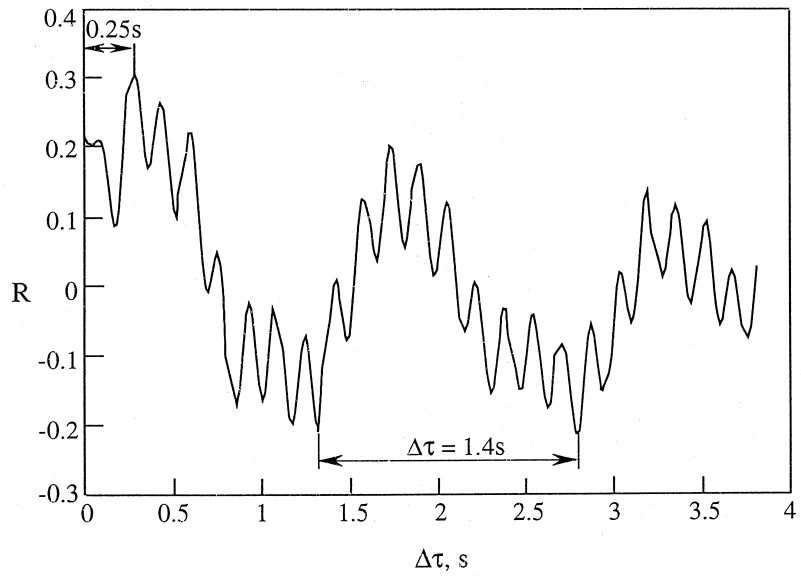

Fig. 6. Cross-correlations of pressure signals: (a) bubble flow ($Re_L = 16{,}000$; $V_{GS}/V_{LS} = 0.08$); (b) slug flow ($Re_L = 16{,}000$; $V_{GS}/V_{LS} = 1.15$).

Alternatively, it is possible just to find the period of cross-correlation function, as a time between two neighboring maxima.

These experimental data agree fairly well with the values of characteristic frequency for both the bubble and the slug flow. The simplest calculation, based on the data of the cross-correlation curves shows that the characteristic frequencies, depending on the calculation method, are 6.05 and 5.56 Hz at experimental value 5.7 Hz for bubble flow, and 0.85 and 0.71 Hz at experimental value 0.7 Hz. This emphasizes the significance of the pressure propagation velocity for the study of two-phase flows.

The intensity of the pressure fluctuation can be estimated by its std value. In Fig. 7, the std of the pressure fluctuations is shown as depending on the value V_{GS}/V_{LS}, where V_{GS}, V_{LS} are superficial velocities of air and water, respectively, Table 1. Below, we will use this form of velocity ratio, because most of the heat transfer data from the literature were given in the same way. We normalized the fluctuation value by the level of the pressure fluctuations at the wall without air. This level is determined by the turbulent fluctuations level with negligible amount of air in the water. Fig. 7 is similar to that described by Tutu (1984). In both cases the value of the std of the pressure fluctuations changes a little at bubble flow and increases at slug flow.

3.2. Thermal structure and temperature fluctuations

Several maps of two-phase flow patterns have been proposed (see e.g. Taitel et al., 1980; Ohnuki and Akimoto, 1996). Undoubtedly, the heat transfer and wall temperature fluctuations depend on the flow pattern. However, there are no data on how flow parameters are related to the near-wall flow structure, which determines the heat transfer coefficient. Our IR visualization method sheds additional light on this phenomenon.

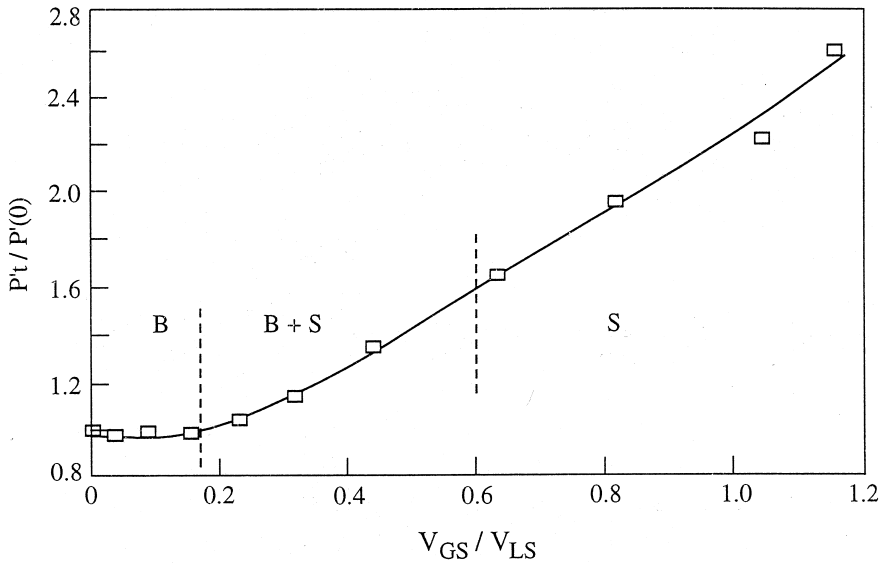

Fig. 7. The std pressure fluctuations as a function of superficial velocities ratio. (B, bubble flow; B + S, bubble + slug flow; S, slug flow).

Table 1

Superficial velocity (m/s)		$\mathrm{Re}_L = \frac{V_{LS} \times d}{\nu}$	$\mathrm{Fr} = \frac{V_{LS}}{\sqrt{gd}}$	$q \times 10^{-3}$ W/m^2
Water	Air			
0.08–0.74	0–0.195	6800–63,000	0.094–0.87	1.9–23.5

The typical IR images of the heated wall of the test section at various regimes of air–water flow are shown in Fig. 8. Fig. 8(a) shows the streaky structure of the clear water turbulent flow. The thermal streaks in the horizontal channel were described by Moffat (1990), Iritani et al. (1983, liquid crystal method) and by Hetsroni and Rozenblit (1994, IR technique method). The thermal streaks are oriented in the streamwise direction. They move slowly in the downstream direction and migrate simultaneously in the spanwise direction. The movement of the thermal streaks is accompanied by their twisting and merging with the neighboring ones.

The flow structure is drastically changed in the bubble flow regime (Fig. 9(a)). In this case, the gas phase is approximately uniformly distributed in the form of discrete bubbles in a continuous liquid phase. The bubbles interact with the near-wall turbulent boundary layer, which leads to destruction of the near-wall structures. Naturally, the pattern of thermal streaks on the heated wall is destroyed, too. The color play of this picture (Fig. 8(b)) is narrower than that for the streaky structure of the turbulent flow. The quantitative decrease of the std temperature fluctuation at bubble flow is shown in Figs. 10 and 11.

In the slug flow (see e.g. Taitel et al., 1980) most of the gas is located in large bullet-shaped bubbles (“Taylor bubbles”, see Fig. 9(c)), which have a diameter almost equal to the pipe diameter. Between the bubbles and the pipe wall, liquid flows downward in the form of a thin falling film. Along the pipe the bubbles are separated by slugs of continuous liquid containing small gas bubbles (Fig. 9(b)). The thermal pattern on the wall for the slug flow regime has a dual character, too. The temperature distribution depends strongly on whether a Taylor bubble or a liquid containing small bubbles passes the test section at any instant. Fig. 8(c) depicts the thermal distribution on the heated wall when the liquid containing small gas bubbles (slug) passes the heater. The temperature field is very smooth. The spatial difference between different points of the heater does not exceed 0.3°C. However, the thermal distribution is immediately changed when a Taylor bubble passes the heater level. The liquid around the bubble creates, flowing downward, conditions for a streaky structure appearance. This structure has temporal and faint character. Nevertheless, the streaks lead to the existence of a certain level of temperature fluctuations. This level does almost not change in the fully developed slug flow (Figs. 10 and 11). This fact allows us to consider the problem of the heat transfer from the point of view of the limit value of heat transfer coefficient at slug flow.

3.3. Heat transfer in the bubble–slug flow

Several correlations have been used for two-phase heat transfer coefficients. Kudirka et al. (1965) and Dorresteijn (1970) correlated the heat transfer enhancement $\eta = \alpha/\alpha_L$ over single-phase liquid heat transfer. Vijay et al. (1982) developed correlations based on the Lockhart–

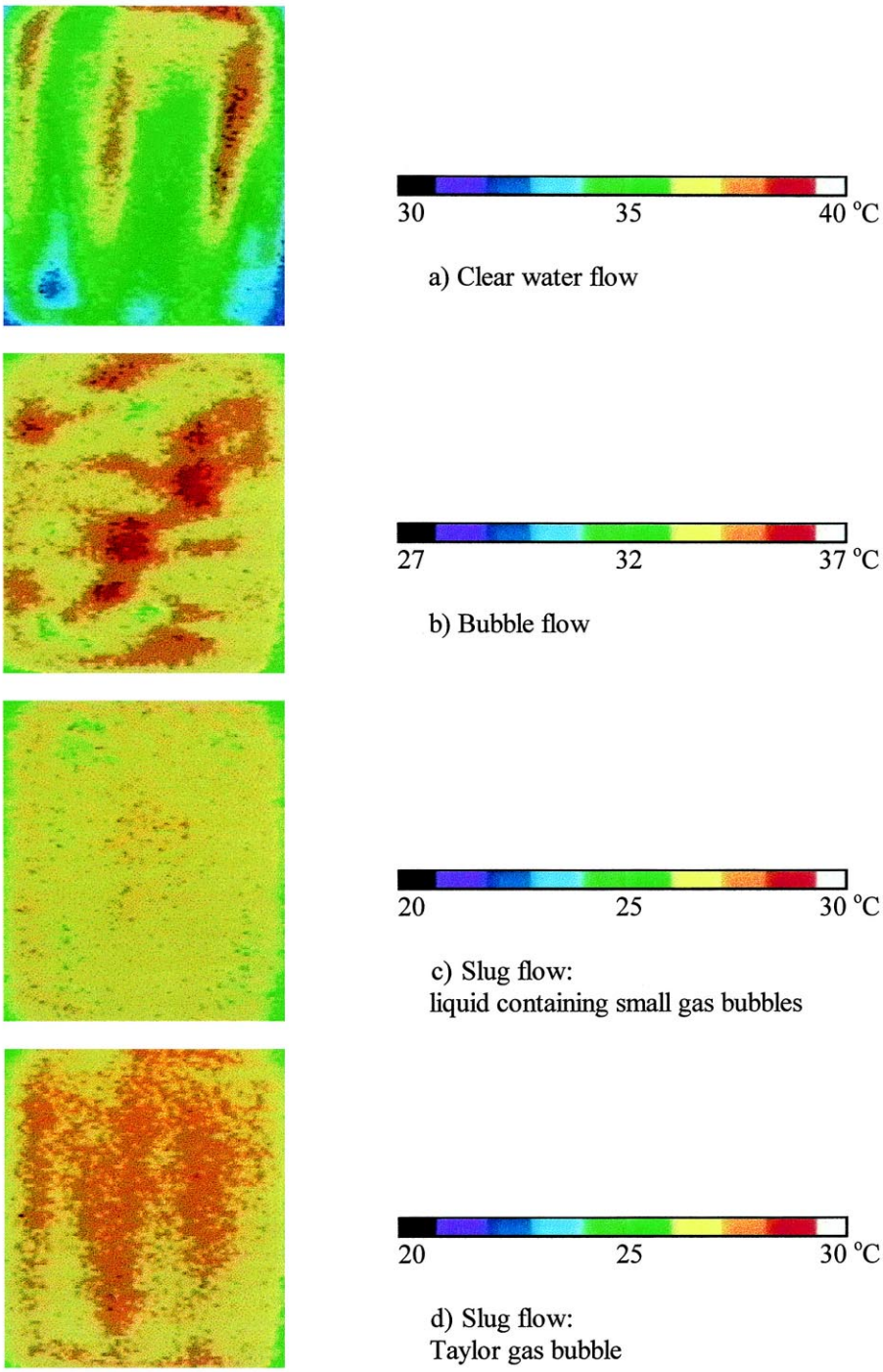

Fig. 8. The typical IR images of the heated wall of the test section at various flow regimes (Re = 8200; $T_f = 25°C$; real image dimensions are 8 × 6 cm).

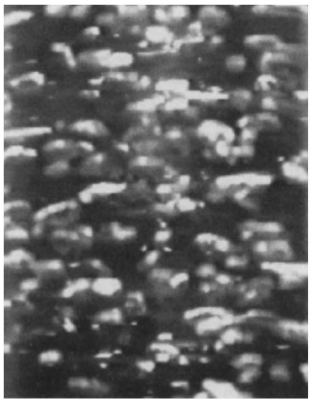

a) Bubble flow

b) Slug flow: liquid containing small gas bubbles

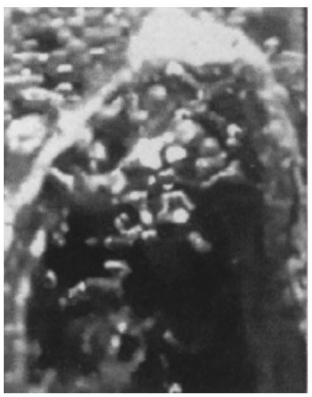

c) Slug flow: Taylor gas bubble

Fig. 9. The typical video images of flow structure at various flow regimes ($Re_L = 8200$; real image dimensions are 10×7.4 cm).

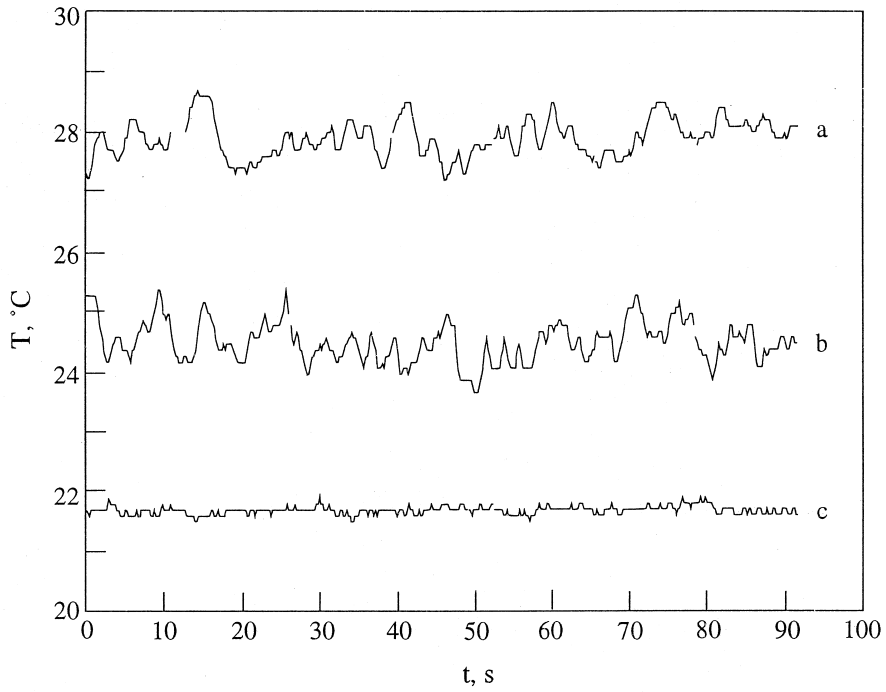

Fig. 10. The typical temperature signals at various flow regimes. $Re_L = 16{,}000$; q = 12,000 W/m^2. (a) Clear turbulent water flow; (b) bubble flow, $V_{GS}/V_{LS} = 0.034$; (c) slug flow, $V_{GS}/V_{LS} = 1.04$.

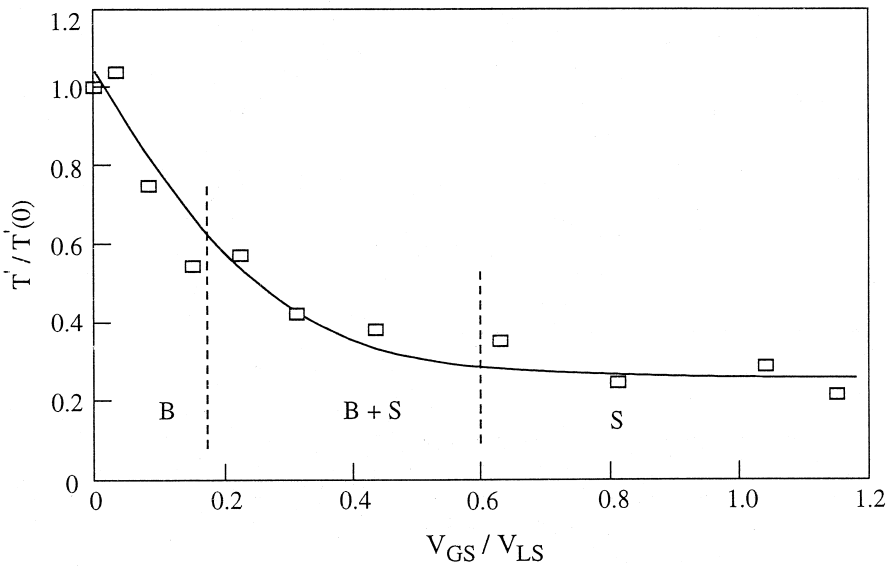

Fig. 11. The std temperature fluctuations as a function of the superficial velocities ratio. $Re_L = 16{,}000$; q = 12,000 W/m^2 (B, bubble flow; B + S, bubble + slug flow; S, slug flow).

Martinelly parameter $\phi^2_L = \Delta p/\Delta p_L$. The values of single-phase liquid heat transfer coefficient α_L and pressure drop Δp_L are determined from standard heat transfer and friction factor correlations. The correlations in the form of a modification of the Sieder–Tate equation were proposed by Groothuis and Hendal (1959), Ravipudi and Godbold (1978), and Elamvaluthi and Srinivas (1983). In these works, the heat transfer experimental data and the data and correlations from various sources were compared. It can be seen that there is a considerable deviation of the experimental data from the available correlations. This fact demonstrates the lack of comprehension of heat transfer at different flow regimes of two-phase flow.

Most of the experimental data of various sources (Fig. 12) have a flat part of the curves which present the dimensionless heat transfer coefficient α/α_L, depending on the ratio of superficial velocities V_{GS}/V_{LS} at a vertical slug flow regime. A similar behavior of the average dimensionless heat transfer coefficient was found in horizontal tubes (Johnson and Abou-Sabe, 1952) at relatively high values of V_{GS}/V_{LS}. However, local values of the coefficient on the upper part of a horizontal tube at low Re_G (intermittent flow) may be several times lower than

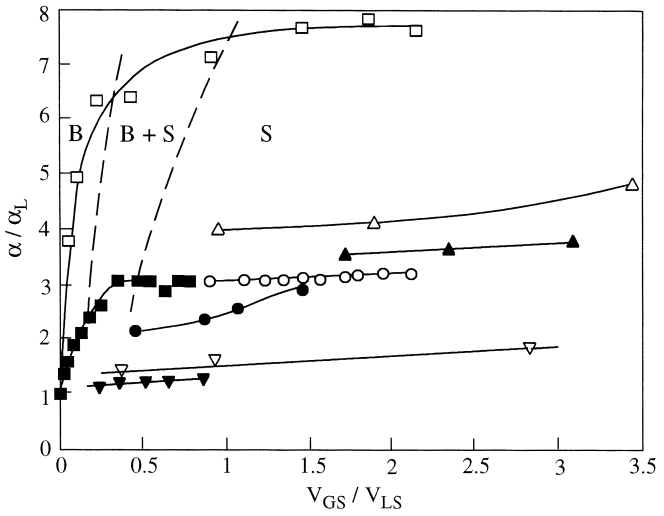

Symbol	Source	System	u_L m/s	Tube I.D. cm
○	Chu & Jones (1980)	air-water	0.42	2.67
△	Groothuis & Handel (1959)	air-oil	0.50	1.4
▲	Elamvaluthi & Srinivas (1984)	air-glycerine	0.50	1.0
●	Elamvaluthi & Srinivas (1984)	air-water	1.1	1.0
□	Present	air-water	0.08	7.4
■	Present	air-water	0.31	7.4
▽	Kudirka et al. (1965)	air-water	1.37	1.6
▼	Kudirka et al. (1965)	air-water	2.73	1.6

Fig. 12. The dimensionless heat transfer coefficient vs the superficial velocities ratio (B, bubble flow; B+S, bubble+slug flow; S, slug flow).

those for the clean water flow, while these values are practically independent of the superficial gas velocity on the lower part of the tube (Kago et al., 1986; Hetsroni et al., 1998a,b). On the other hand, even a small (2–5°) upward inclination of the tube causes the local heat transfer coefficients on the upper part to increase and approach the values on the lower part (Hetsroni et al., 1998a,b), because of increasing influence of bubble-induced turbulence on heat transfer.

Consider the data on fluctuating values of the pressure and temperature and thermal patterns on the vertical wall. The strong pressure fluctuations at the wall in the slug flow regime destroy completely the near-wall turbulent structure. The statistical properties of these mainly bimodal form fluctuations have a normal-law character. This form of oscillation smoothes the temperature distribution at the wall. The level of the temperature fluctuations almost does not depend (Figs. 10 and 11) on the superficial velocities ratio. This level is very small and is determined by the short time of streaky structure regeneration. It is natural under these conditions to introduce the excess heat transfer coefficient $\bar{\alpha}_{ex}=(\alpha-\alpha_L)/(\alpha_{SLUG}-\alpha_L)$ where α, α_L and α_{SLUG} are heat transfer coefficients for given conditions, clear water, and slug flow, respectively, at a given Reynolds number $Re=V_{LS}\ d/\nu$. The excess heat transfer coefficient equals unity for the slug flow and zero for clear liquid. Fig. 13 shows our experimental data in that form. It can be seen that curves at different values of the Reynolds number converge in single curve.

The excess heat transfer coefficient contains the value of the heat transfer coefficient α_L for the liquid without gas phase. The magnitude of α_L can be found from the Sieder–Tate equation or in the other form (e.g. Holman, 1989) as

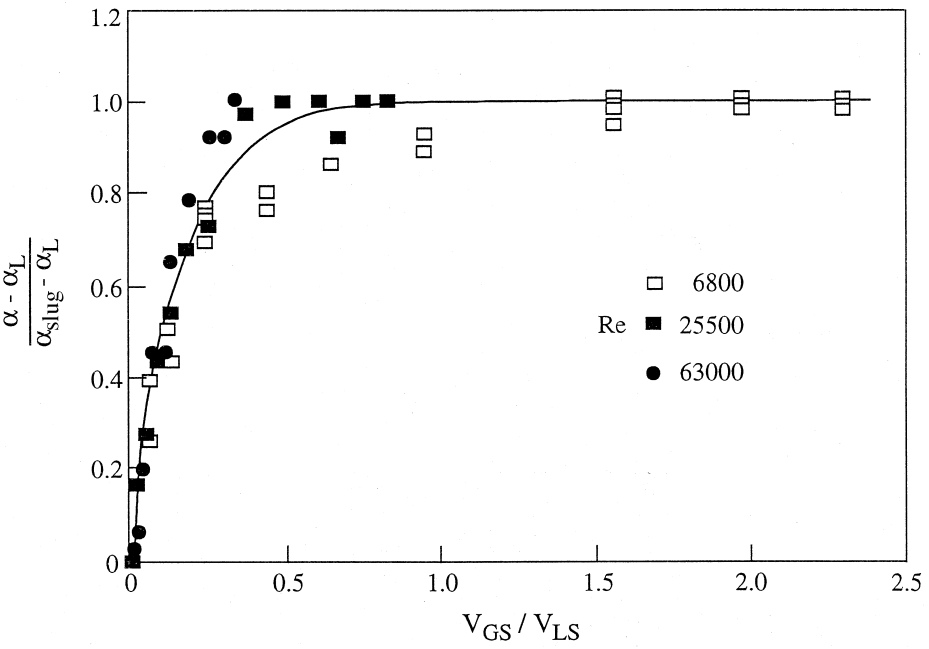

Fig. 13. Excess heat transfer coefficient.

$$\mathrm{Nu}_L = 0.023\mathrm{Re}^{0.8}\mathrm{Pr}^{0.4} \tag{7}$$

where $\mathrm{Nu}_L = \alpha_L\ \mathrm{d}/\lambda$ is the Nusselt number. We used, following Tutu (1984), the Reynolds number and the Froude number $\mathrm{Fr} = V_{LS}/(gd)^{0.5}$ based on the liquid superficial velocity for the data generalization on the heat transfer coefficient at slug flow regime.

In Fig. 14, the data of various sources are presented on the limit values of heat transfer coefficients at slug flow in coordinates α/α_L, $\mathrm{ReFr}^{0.5}$. The second coordinate $\mathrm{ReFr}^{0.5}$ has been found by best fitting the powers to the Re and Fr numbers.

For the data presented here

$$\alpha_{\mathrm{SLUG}}/\alpha_L = 141.1\mathrm{Re}^{-0.4}\mathrm{Fr}^{-0.2} \tag{8}$$

or using the correlation (7), we have

$$\mathrm{Nu}_{\mathrm{SLUG}} = 3.25\mathrm{Pe}^{0.4}\mathrm{Fr}^{-0.2} \tag{9}$$

where $\mathrm{Pe} = V_{LS}\ \mathrm{d}/a$ is the Peclet number, a is the thermal diffusivity.

Thus in the developed air–water slug flow, when the turbulent boundary layer is completely

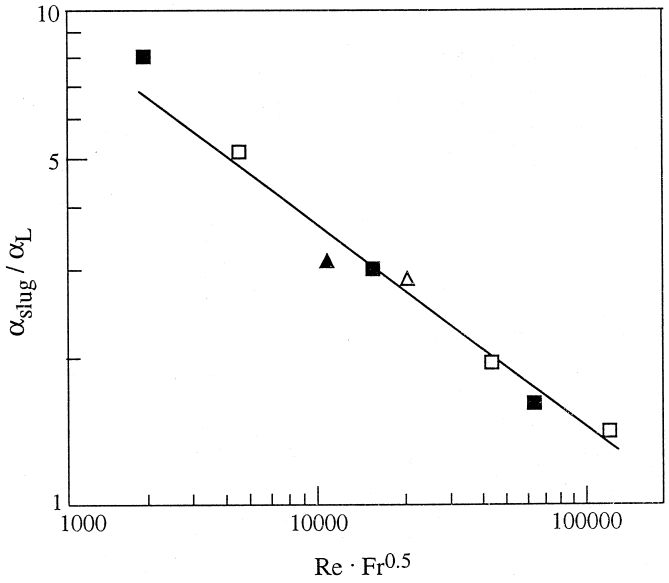

Symbol	Source
■	Present
▲	Chu & Jones (1980)
□	Kudirka et al. (1965)
△	Elamvaluthi & Srinivas (1984)

Fig. 14. The dimensionless heat transfer coefficient at air–water slug flow vs ReFr^{05}.

destroyed and the flow is intermittent, the heat transfer coefficient is determined by the Peclet and Froude numbers.

4. Conclusions

The temperature patterns on the heated wall, as related to the flow structure, were studied using the heated foil infrared technique. Simultaneously, the temperature and pressure fluctuations at the wall were measured. The character of fluctuating values was analysed by using power spectral density and probability density functions. The characteristic frequencies were found by estimating the cross-correlation of two pressure signals. The level of fluctuations of the pressure and the temperature was qualitatively discussed together with the data about the average heat transfer.

The thermal pattern on the heated wall for the single-phase water flow has a streaky structure similar to the turbulent structure in a horizontal pipe or channel flow.

For the bubble flow, the streaky structure is destroyed. This phenomenon is accompanied by a significant increase in the heat transfer coefficient and sharp decrease in the temperature fluctuation values, whereas the level of pressure fluctuations at the wall almost did not change. The pressure fluctuations have an almost periodic character. The frequency of pressure fluctuation is related to the propagation velocity and the pipe height.

For the slug flow regime, the thermal pattern on the wall is quite different. The temperature distribution on the heated wall depends strongly on whether water containing small gas bubbles (slug) or water surrounding the Taylor bubble passes the heated wall at any instant. For the first case the temperature field is very smooth, whereas for the second case the streaky structure appears as the water around the Taylor bubble flowing downward creates conditions for its regeneration. The level of the pressure fluctuation increases when V_{GS}/V_{LS} increases, whereas the level of the temperature fluctuations almost does not change at slug flow, and is determined by a temporal character of the structure regeneration. The statistical properties of the pressure fluctuations have a normal distribution.

The excess form of the heat transfer coefficient was introduced. This form originates from a consideration of thermal patterns on a heated wall, as well as from independence of the dimensionless heat transfer coefficient in slug flow on the ratio V_{GS}/V_{LS}. It was found that the magnitude of the heat transfer coefficient at slug flow is related to the Peclet and Froude numbers.

Acknowledgements

This research was supported by a grant from the Ministry of Science; by the Technion VPR fund. This research is also supported by a grant from the German Federal Ministry of Education, Science, Research and Technology (BMBF) and the Israeli Ministry of Science (MOS). R. Rozenblit is partially supported by the Center for Absorption in Science, Ministry of Immigrants Absorption, State of Israel.

References

Baba, N., Yamashita, Y., Shiraishi, Y., 1991. Classification of flow patterns in two-phase flow by neural networks. Proc. IEEE Int. Conf. Neural. Netw 2, 2617–2620.

Chu, Y.C., Jones, B.G., 1980. Convective heat transfer coefficient studies in upward and downward vortical, two-phase, non-boiling flows. AIChE Symp. Series 76, 79–90.

Costigan, G., Whalley, P.B., 1997. Slug flow regime identification from dynamic void fraction measurements in vertical air–water flows. Int. J. Multiphase Flow 23, 263–282.

Dorresteijn, W.R., 1970. Experimental study of heat transfer in upward and downward two-phase flow of air and oil through 70 mm tubes. In: Proc. 4th Int. Heat Transfer Conf, 5, p. B5.9.

Dukler, A.E., Taitel, Y., 1986. Flow pattern transitions in gas–liquid systems: measurement and modeling. Multiphase Sci. Technol. 2, 1–94.

Elamvaluthi, G., Srinivas, N.S., 1983. Two-phase heat transfer in two component vertical flows. Int. J. Multiphase Flow 10, 237–242.

Groothuis, H., Hendal, W.P., 1959. Heat transfer in two-phase flow. Chem. Eng. Science 11, 212–220.

Hetsroni, G., Rozenblit, R., 1994. Heat transfer to a liquid–solid mixture in a flume. Int. J. Multiphase Flow 20, 671–689.

Hetsroni, G., Hu, B.G., Yi, J.H., Mosyak, A., Yarin, L.P., Ziskind, G., 1998a. Heat transfer in intermittent air–water flow—Part I: Horizontal tube. Int. J. Multiphase Flow 24, 165–188.

Hetsroni, G., Hu, B.G., Yi, J.H., Mosyak, A., Yarin, L.P., Ziskind, G., 1998b. Heat transfer in intermittent air–water flow—Part II: Upward inclined tube. Int. J. Multiphase Flow 24, 189–212.

Holman, J.P., 1989. Heat Transfer, SI metric ed. McGraw-Hill Book Company.

Hubbard, M.B., Dukler, A.E., 1966. The characterization of flow regimes for horizontal two-phase flow. In: Saad, M.A., Miller, J.A. (Eds.), Proceedings of Heat Transfer and Fluid Mech. Inst. Stanford University Press.

Iritani, Y., Kasagi, N., Hirata, M., 1983. Heat transfer mechanism and associated turbulent structure in the near-wall region of a turbulent boundary layer. Turbulent Shear Flows IV, 223–234.

Johnson, H.A., Abou-Sabe, A.H., 1952. Heat transfer and pressure drop for turbulent flow of air–water mixtures in a horizontal pipe. Transition of the ASME 977–987.

Jones, O.C., Zuber, N., 1975. The interrelation between void fraction fluctuations and flow patterns in two-phase flow. Int. J. Multiphase flow 2, 273–306.

Kago, T., Saruwatari, T., Kashima, M., Morooka, S., Kato, Y., 1986. Heat transfer in horizontal plug and slug flow for gas–liquid and gas–slurry systems. Journal of Chemical Engineering of Japan 19, 125–131.

Kosaly, G., Albrecht, R.W., Crowe, R.D., Dailey, D.J., 1982. Neutronic response to two-phase flow in a nuclear reactor. Prog. Nucl. Energy 9, 23–36.

Kozma, R., Kok, H., Sakuma, M., Djainal, D.D., Kitamura, M., 1996. Characterization of two-phase flows using fractal analysis of local temperature fluctuations. Int. J. Multiphase Flow 22, 953–968.

Kudirka, A.A., Grosh, R.J., McFadden, P.W., 1965. Heat transfer in two-phase flow of gas–liquid mixtures. Ind. Eng. Chem. Fundam. 4, 339–344.

Moffat, R.J., 1990. Experimental heat transfer. In: Hetsroni, G. (Ed.), Proceedings of the Ninth International Heat Transfer Conference, Hemisphere, New York, pp. 187–205.

Ohnuki, A., Akimoto, H., 1996. An experimental study on developing air–water two-phase flow along a large vertical pipe: effect of air injection method. Int. J. Multiphase Flow 22, 1143–1154.

Ravipudi, S.R., Godbold, T.M., 1978. The effect of mass transfer on heat transfer rates for two-phase flow in a vertical pipe. In: Proceedings of the 6th International Heat Transfer Conference, Toronto, vol. 1, pp. 505–510.

Taitel, Y., Barnea, D., Dukler, A.E., 1980. Modeling flow pattern transitions for steady upward gas–liquid flow in vertical tubes. AIChE Journal 26, 345–354.

Tutu, N.K., 1984. Pressure drop fluctuations and bubble–slug transition in a vertical two-phase air–water flow. Int. J. Multiphase Flow 10, 211–216.

Vijay, M.M., Aggour, M.A., Sims, G.E., 1982. A correlation of mean heat-transfer coefficients for two-phase, two-component flow in a vertical tube. In: Proceedings of the 7th International Heat Transfer Conference, Munich, vol. 5, pp. 367–372.

Vince, M.A., Lahey, R.T., 1982. On the development of an objective flow regime indicator. Int. J. Multiphase Flow 8, 93–124.

Wallis, G.B., 1969. One Dimensional Two-Phase Flow. McGraw-Hill.

Zuber, N., Staub, F.W., 1967. An analytical investigation of the transient response of the volumetric concentration in a boiling forced-flow system. Nucl. Sci. Eng 30, 268–278.